40th AIAA Plasmadynamics and Lasers Conference
22 - 25 June 2009, San Antonio, Texas

AIAA 2009-4226

40th AIAA Plasmadynamics and Laser Conference
San Antonio, Texas, 22-25 Jun, 2009

Obtaining Velocity Distribution using a Xenon Ion Line with Unknown Hyperfine Constants

Wensheng Huang [*], Timothy B. Smith[†], and Alec D. Gallimore[‡]
Plasmadynamics and Electric Propulsion Laboratory, University of Michigan,
1919 Green Rd Rm B107, Ann Arbor, MI 48109, 734-764-4199

We present and validate a method for extracting velocity distribution functions from laser-induced fluorescence measurements obtained using a xenon ion line with unknown hyperfine constants. The method involves a direct deconvolution of intermodulated experimental results from the laser-induced fluorescence measurements. The intermodulated experiments were done on the $5d[4]_{7/2} \rightarrow 6p[3]^{o}_{5/2}$ transition for singly-charged xenon at 834.7 nm. The hyperfine constants for this line are large enough to distort the results but small enough to have eluded accurate measurement. This approach is validated using both simulated results and a set of measurements taken in a Hall thruster environment. The validity of the method is scrutinized through the uncertainty analysis that follows. The method was determined to contribute at most ±0.1% to the absolute uncertainty of the velocities and at most a 4% decrease to the full-width-at-half-maximum of the velocity distribution functions measured in the accelerating plasma of the Hall thruster.

I. Introduction

THE Hall thruster is an excellent propulsive device for interplanetary mission and station keeping because of its high specific impulse (1000's of seconds), high efficiency (50-60%), and engineering scalability (200 W-100 kW). A full understanding of the inner workings of a Hall thruster remains beyond our grasp due to a lack of internal and near field data. Laser-induced fluorescence (LIF) presents a non-intrusive, specifies-specific, spatially-resolved approach to obtaining velocity distribution function (VDF) from the plasma inside a Hall thruster.

The singly-charged xenon $5d[4]_{7/2} \rightarrow 6p[3]^{o}_{5/2}$ transition at a wavelength of 834.7 nm in air has been previously used via LIF to obtain VDF in Hall thruster diagnostics.[1-6] This transition presents several advantages over other ion transitions. First, commercial high-power continuous-wave diode lasers are available at this wavelength. Second, its lower state is metastable so a large lower state population exists in highly energetic systems like Hall thrusters. And third, its upper state has a strong non-resonant transition at 541.9 nm so scattering effect is not an issue. However, using this transition does have one major drawback; the lower state hyperfine structure constants are not known. Smith et al. attempted to find these constants via a conjugated gradient solver,[2] but the noise in the data and the Doppler broadening made it possible for the solution to be non-unique. Mazouffre et al. attempted a Lamb-dip experiment but their results do not show clearly identifiable spikes. Their analysis is still ongoing as of the writing of this paper.[7]

Due to the lack of a definitive experiment that resolves the hyperfine constants for this transition, past LIF experiments have either used the most probable velocity to characterize the results[3] or simply did not deconvolve the hyperfine structure out of the result and accepted higher uncertainty.[6] These approaches are acceptable in a Hall thruster environment for analyzing bulk trends of velocity distribution functions for two reasons. First, due to plasma oscillations in Hall thrusters and Doppler broadening, raw traces typically appear to be much broader than the hyperfine structure for this transition. Second, the uncertainty is often dominated by noise from the plasma oscillations, so that uncertainty associated with hyperfine structures is typically small in comparison.

However, many important effects like charge-exchange and partial ion acceleration show up as tails in the velocity distributions. The accuracy with which the magnitude of these low-lying populations can be calculated is highly dependent on properly deconvolving out the hyperfine structure. Furthermore, relatively quiet regions of the Hall thruster plasma, such as upstream of the acceleration zone, tend to have fairly narrow velocity distributions.

---

[*] Ph. D. Candidate, Aerospace Engineering, davhuang@umich.edu, Student Member, AIAA.
[†] Research Fellow and Lecturer, Aerospace Engineering, timsmith@umich.edu, Senior Member, AIAA.
[‡] Arthur F. Thurnau Professor, Aerospace Engineering, alec.gallimore@umich.edu, Associate Fellow, AIAA.

Not accounting for the effect of hyperfine structure constants will yield inaccurate width measurements and therefore incorrect temperatures. These effects are particularly important for experiments with high signal-to-noise (SNR) ratios, where the uncertainty can be dominated by the hyperfine structure effects.

The standard approach to removing the effects of hyperfine structure is to create a hyperfine lineshape based on quantum theory using known constants, and convolve it with broadening profiles like natural broadening, the laser frequency profile, and other relevant factors except the Doppler shift. This approach then uses any of a number of mathematical/numerical approaches to deconvolve the resulting lineshape from the raw LIF trace to obtain the Doppler-shifted component, which is the VDF. The rest of this paper will discuss a series of intermodulated experiments to obtain the said convolved lineshape, bypassing the need to know the hyperfine structure constants. Then, the paper will validate the VDFs obtained by direct deconvolution in an uncertainty analysis. This method is not restricted to this particular transition but can be applied to other transitions used in similar situations.

II. Theories

Sections A-C lay out the theory underlying the extraction of VDFs from raw LIF spectra. Section D describes the phenomenon known as saturation and the saturation-based technique for extracting Doppler-free spectra called intermodulated optogalvanic spectroscopy (IMOG). Note that for the remainder of the paper, all transition wavelengths are given in air values and all intensities given in arbitrary units, a.u., unless otherwise specified. Full-width-at-half-maximum (FWHM) values are used instead of temperature to describe the width of the velocity distributions found in the plume of the Hall thruster because Hall thruster plasma is typically non-Maxwellian. Also, the signal-to-noise ratio (SNR) in this paper is defined as the amplitude of the tallest spectral peak divided by the amplitude of the noise; this definition ensures that the SNR is independent of the intensity scaling.

A. Principles of Laser-Induced Fluorescence Velocimetry

LIF operates on the principle that when a particle (an atom or molecule) absorbs a photon, it will de-excite and emit another photon. Excited particles will de-excite by collision, spontaneous emission, or stimulated emission. Particles that spontaneously emit photons at the same energy as the absorbed photons are said to undergo resonant emission. Particles that emit photons at energies different from that of the absorbed photons are said to undergo non-resonant emission. This spontaneous emission, called fluorescence, radiates isotropically away from the particle.

To obtain the particle velocity distribution via LIF, we take advantage of the Doppler shift. For a particle travelling at non-relativistic speed, the shift in absorption frequency is proportional to the particle velocity component in the direction that the photon travels. The mathematical equation is given by

$$\frac{\Delta\upsilon}{\upsilon_0} = -\frac{\mathbf{v}}{c}\cdot\frac{\mathbf{k}}{|\mathbf{k}|} \tag{1}$$

where υ_0 is the photon frequency, $\Delta\upsilon$ is the shift in photon frequency from the perspective of the particle, $\mathbf{v}$ is the particle velocity, c is the speed of light, and $\mathbf{k}$ is the photon wave vector. By varying the frequency of the injected photons and comparing the intensity of the collected fluorescence, we can obtain the particle VDF along the injected photon wave vector. For the data collected to validate the methodology in this paper, light is injected at around 834.7 nm and non-resonant LIF is collected at 541.915 nm.

Note that when an atom in the lower energy state absorbs a photon and rises up to a higher energy state, it is also more likely to get ionized. Instead of measuring the fluorescence, one can measure the extra current created by the laser-induced excitation to yield spectral lineshapes. This is called optogalvanic spectroscopy.

B. Hyperfine Structure and Natural Broadening

The FWHM of the average ion VDF in a Hall thruster typically varies from 800 to 2500 m/s, which for a near-infrared transition corresponds to about 1000 to 3000 MHz. Unfortunately, xenon hyperfine structures typically have frequency shifts of 10s to 1000s of MHz. These structures can add large distortions to the raw data. This effect shows up as multiple distinct spikes in a cold (T = 0 K) spectrum where there would normally only be one spike. Hyperfine structure is a result of two atomic level effects. The first effect is due to the interaction between the nuclear electric and magnetic moments with the electronic angular momentum. The second effect, called the isotopic shift, is due to minute differences in the masses and electron orbital shapes of different isotopes. This topic is dealt with in greater detail by Svanberg.[8]

Unfortunately, the hyperfine splittings for the Xe II $5d[4]_{7/2} \rightarrow 6p[3]^{o}_{5/2}$ transition are large enough to broaden the raw lineshape but small enough such that no accurate determination of the lower state hyperfine structure constants have been made. The upper state constants have been measured via other transitions. Although these constants can be predicted by quantum theory, complexity associated with the many electron orbitals in a xenon atom makes such determination computationally impossible with current knowledge. Without experimentally-derived constants, we need an alternate approach to construct the hyperfine structure lineshape needed to extract velocity distributions from laser-induced fluorescence data. One such approach is called intermodulated spectroscopy, the optogalvanic version of which is described in Section D.

In addition, external electric and magnetic fields can alter the energies of otherwise degenerate states, creating an even greater number of hyperfine splittings. The electric field effect is called the Stark Effect and the magnetic field effect is called the Zeeman Effect. For the LIF data collected to validate the methodology, both types of distortions were avoided. The electric field present in a typical Hall thruster is several orders of magnitude smaller than what is necessary to make the Stark Effect noticeable.[9] The Zeeman Effect, which is applicable for weak magnetic fields (~100 Gauss), can be categorized under σ- and π-polarization. The beam is σ-polarized if the polarization of the beam is perpendicular to the external magnetic field ($\mathbf{E} \perp \mathbf{B}$). The beam is π-polarized if the polarization of the beam is parallel to the external magnetic field ($\mathbf{E} \parallel \mathbf{B}$). For the Xe II $5d[4]_{7/2} \rightarrow 6p[3]^{o}_{5/2}$ transition, π-polarized splittings are at least an order of magnitude narrower than σ-polarized splittings.[10] By injecting the laser beam with π-polarization with respect to the local magnetic field, we obtained LIF scans with negligible Zeeman splitting.[10]

Natural (or lifetime) broadening is a result of the Heisenberg uncertainty principle. Since energy and temporal measurements are complementary, one cannot know with absolute certainty the exact energy of a photon emitted from a particle whose decay time is uncertain. The result is that even if all other circumstances are equal, no two photons from the same de-excitation will be measured with exactly the same energy. This effect broadens a transition line, modeled in frequency space as a Dirac delta function, into a Lorentzian function.[8] Natural broadening for xenon ion line is on the order of tens of MHz, which is typically negligible compared to the effect of hyperfine structures.

A raw LIF spectrum is a result of combining all of the above effects with the velocity distribution function and the laser spectrum function. For the continuous-wave diode laser used in this experiment, the FWHM of the laser spectrum is ~20 MHz, which is on the order of the data resolution. Thus, the laser spectrum has negligible influence on the raw LIF spectrum and can be ignored. To obtain the velocity distribution function, we need to remove, or deconvolve, the above effects from the raw LIF spectrum.

C. Principles of Deconvolution

Deconvolution is a mathematical process that we can use to extract the particle VDF from a raw LIF spectrum. Ignoring noise and other non-ideal effects, the lineshape in frequency space for a species with hyperfine structures can be written as

$$\mathrm{i}(\upsilon) = \mathrm{h}(\upsilon) \otimes \mathrm{nat}(\upsilon) \otimes \mathrm{g}(\upsilon) \tag{2}$$

where $\mathrm{h}(\upsilon)$ is the hyperfine structure function, $\mathrm{nat}(\upsilon)$ is the natural broadening function, and $\mathrm{g}(\upsilon)$ is the VDF in frequency space. A raw LIF spectrum takes on the shape of $\mathrm{i}(\upsilon)$, called the lineshape. The ⊗ symbol represents the mathematical process called convolution, which is defined as

$$C(x) = \int_{-\infty}^{\infty} A(x-y)B(y)dy \tag{3}$$

where the function C is the result of the convolution and the function A is said to be convolved with the function B.

To obtain one of the original components of a convolved function, we employ the deconvolution process, which is the inverse of the convolution process and is represented by the ∅ symbol. Equation (4) shows how the VDF, $\mathrm{g}(\upsilon)$, can be extracted from a raw LIF spectrum, $\mathrm{i}(\upsilon)$

$$\mathrm{g}(\upsilon) = \mathrm{i}(\upsilon) \varnothing \left[\mathrm{h}(\upsilon) \otimes \mathrm{nat}(\upsilon)\right] \tag{4}$$

where $\mathrm{h}(\upsilon) \otimes \mathrm{nat}(\upsilon)$ is also called the kernel. Typically, the kernel is constructed from knowledge of the hyperfine structure constants and the lifetime constant of the transition in question.

Graphically, convolution and deconvolution are both highly intuitive processes. Figure 1 shows an example of convolution represented by Eq. (2) for a typical xenon transition.

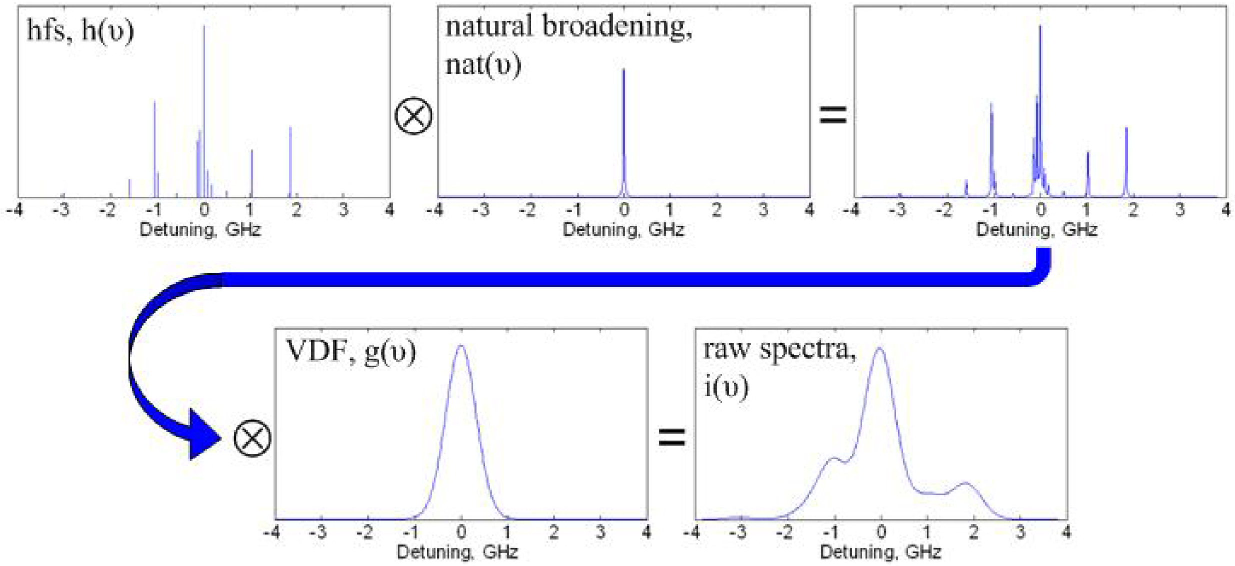

Figure 1. Graphical example of convolution for a typical xenon ion transition.

D. Principles of Intermodulated Optogalvanic Spectroscopy

To obtain the kernel of deconvolution without finding the hyperfine structure and lifetime constants, we turn to a Doppler-free spectroscopic technique. Intermodulated optogalvanic spectroscopy (IMOG) is based on a nonlinear LIF effect called saturation. Physically, saturation happens when the beam intensity is high enough such that excited particles do not have enough time to de-excite before they are struck by another photon. At low input beam intensity, the spontaneous emission rate is proportional to the intensity. But as intensity increases, spontaneous emission rate will increase less and less with intensity until the emission rate asymptotically reaches a maximum. At this point, the recorded emission signal becomes independent of the input beam intensity. This effect holds true for both fluorescence and optogalvanic signals. For a two-level system, saturation can be modeled by

$$I_R \propto \frac{S(\upsilon)}{1+S(\upsilon)}, \text{ where } S(\upsilon) \equiv \frac{I_\upsilon}{I_S(\upsilon)} \tag{5}$$

where I_R is the response (LIF or optogalvanic) of the sampled population, S is called the saturation parameter, I_υ is the injected beam intensity, and I_S is the saturation intensity.[8] It can be shown that I_S is the intensity of injected beam necessary to equally populate the upper and lower state of the transition in question. Note that $I_S(\upsilon)$ is frequency dependent and is inversely proportional to the magnitude of the lineshape i(υ). For this reason, S(υ) is proportional to i(υ) and is higher at the peaks and lower at the troughs for a given transition.

Normally, saturation effect is to be avoided because the tendency for peaks to be more saturated than troughs leads to an artificial broadening of the lineshape. However, saturation can be taken advantage of to produce a Doppler-free signal. From Eq. (2), we see that if the Doppler effect, g(υ), is removed, only the kernel remains. In this case, the kernel becomes a Doppler-free scan of the transition being examined. Depending on how well resolved the Doppler-free scan is, hyperfine structure constants and natural linewidth can be approximated.

To carry out IMOG, two laser beams of approximately equal intensity are sent from the opposite directions to converge on the interrogation zone. Normally, one beam interacts with the population travelling one way while the other beam interacts with the population travelling in the opposite direction. When the photon frequency of the beams matches the zero-velocity frequency, both beams interact with the same population. If the interaction is linear, no change occurs in the response of the signal. However, if the intensities of the beams are high enough to produce strong saturation, the total response at the zero-velocity frequency will be different than the response at other frequencies. By modulating (mechanically chopping) the input beams at frequencies f_1 and f_2, respectively, a Doppler-free response is obtained at frequencies f_1+f_2 and f_1-f_2.[8] Note that the modulation frequency refers to the rate at which light is physical blocked and unblocked, and is not to be confused with the wave frequency of the light.

In practice, some Doppler broadening shows up in IMOG spectra due to velocity-changing collisions that re-direct particles to go in the exact opposite direction. In addition, the two beams cannot be perfectly aligned. While these broadening effects are small, so is the Doppler-free signal. Defining the said broadening effects as noise, it can be shown with the saturation model equation, Eq. (5), that the SNR for an IMOG spectrum asymptotically reaches a maximum as the degree of saturation is increased. Note also that for a given total power, the signal theoretically maximizes when that power is equally split between the two beams.

Realistically, the degree of saturation is dependent on the power of the laser and the ability to focus two beams onto the same interrogation volume. Furthermore, an IMOG spectrum is not immune to the same undesirable broadening effect that can be found in LIF and regular optogalvanic traces. This effect is part of the reason why normally IMOG is only used to extract the hyperfine constants and the kernel is constructed from those constants. For the purpose of this experiment, the saturation broadening effect puts an additional lower limit on the obtained kernel line width. The thinner the kernel line width, the closer it is to being Doppler-free.

IMOG uses an optogalvanic cell as the response collection device. The cell is an enclosed space with the sample gas and two closely-spaced hollow electrodes inside. This design creates a quiet, well-behaved plasma. Intermodulated experiments performed in an optogalvanic cell can result in very high SNR.

III. Experimental Apparatus and Procedures

A. Experimental Setup A

Figure 2 shows the laser and optics setup for what would become the first of two IMOG experiments. Two relatively weak beams are split off from the main laser beam and sent into the etalon assembly and the wavemeter for reference information. The remaining beam is split into pump beam A and pump beam B.

Pump beam A, chopped at ~1160 Hz, was typically ~10% weaker than pump beam B due to limitations in the optics. During the saturation study, a variable density filter and a photodiode (shown in dashed lines) are added while pump beam B is blocked. Both pump beams have a physical cross-sectional diameter of ~1 mm.

Pump beam B is chopped at ~970 Hz using a different set of slots on the same chopper that chops pump beam A. This beam is aligned to overlap with pump beam A in the middle of the optogalvanic cell with the beam axis being within 0.1° of each other.

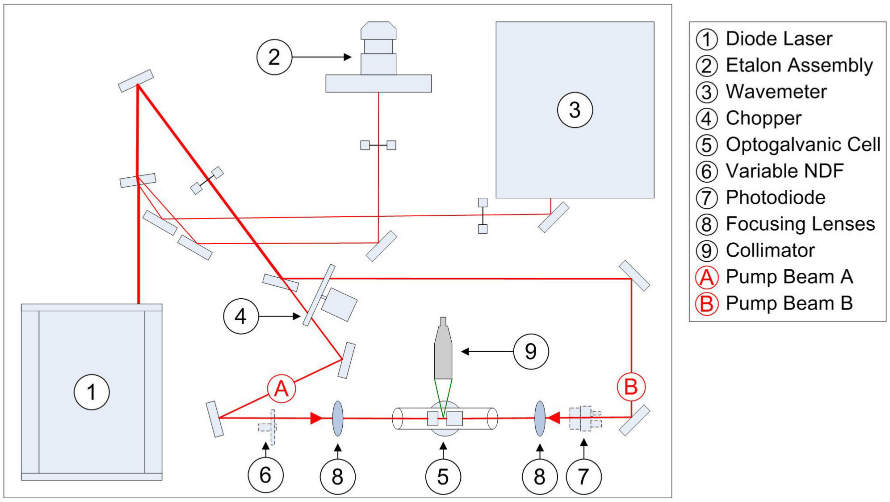

Figure 2. Optical setup for the first IMOG experiment.

A pair of plano-concave focusing lenses designed to focus the beams into a much smaller volume can be added or removed. A collimator focused on the interrogation zone is added to allow fluorescence signal to be collected during the intermodulated tests. An optical fiber brings the fluorescence signal to a SPEX-500M monochromator, the output of which is amplified by a Hamamatsu R928 photomultiplier. The amplified signal is sent to a lock-in amplifier.

The optogalvanic cell used in this study is a Hamamatsu L2783-42 XeNe-Mo galvatron. The core of the galvatron is a pair of φ6.25 mm cylindrical Mo tube electrodes centered in a φ25 mm x 120 mm glass cylinder. The cylinder is filled with approximately 3 torr of xenon and 4 torr of neon. The ends of the cylinder are angled approximately 10 degrees from being perpendicular to the electrode axis to eliminate retro-reflection. This design permits unobstructed passage of a laser beam along the axis shared by the cylinder and electrodes.

The galvatron is operated at 250 V to maintain a warm, dense, and stationary plasma rich with ion species. A ballast resistor prevents runaway current growth after the discharge is struck, and provides a simple method of measuring the discharge current. The voltage drop across the ballast resistor is connected to the SR-810 lock-in amplifier through an RC filter that passes only the AC component of the signal. Data are collected at both the sum and the difference of the two chopping frequencies.

B. Experimental Setup B

Data gained from setup A showed that the limitations imposed by the various noise and saturation effects may give rise to a particular saturation level that yields the best IMOG results. Setup B, shown in Fig. 3, was designed to allow better control of the saturation level. The variable neutral density filter simultaneously changes the power of both pump beams by the same percentage. Fluorescence collection capability was removed because setup A showed that optogalvanic signal collection yielded much higher signal-to-noise ratio.

A few mirrors were removed from the setup in order to increase the maximum power delivered. Better optics management also brought the power of the two pump beams to within ~6% of each other. Chopping frequencies were slightly lower, at ~1140 and ~950 Hz for pump beams A and B, respectively. A saturation study was performed in much the same manner as with setup A. Another photodiode, different from the one used for the saturation study, was added to monitor laser power drift for troubleshooting purpose.

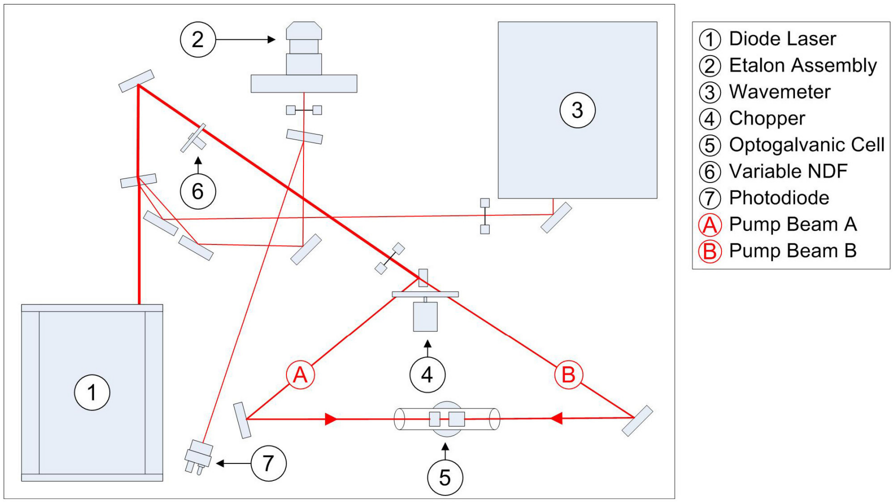

Figure 3. Optical setup for the second IMOG experiment.

IV. Data Analysis and Results

A. IMOG Results versus IM-LIF Results

Since intermodulated spectroscopy has comparatively low signal-to-noise, the first step to mapping out a clean kernel is to try different signal collection methods. Setup A allowed a comparison of intermodulated optogalvanic (IMOG) versus intermodulated-laser-induced fluorescence (IM-LIF) spectroscopy. Also, the focusing lenses made it possible to investigate the effect of changing saturation level without changing total pump beam power.

Figures 4 and 5 show the saturation study plot for optogalvanic and fluorescence collection scheme, respectively. The peak intensity readings have ~3% error and the normalized laser power readings have ~1% error. The laser power was normalized to 25±1 mW; this is the maximum laser power of pump beam A before it enters the optogalvanic cell as measured by a thermopile while the chopper is running. Each figure contains dashed lines fitted

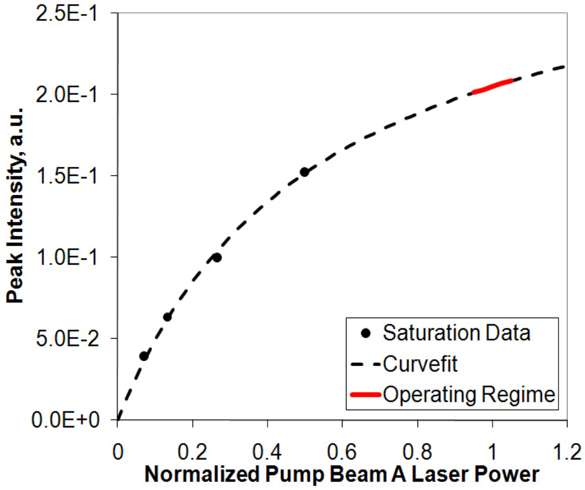

Figure 4. Saturation study plot for IMOG setup A

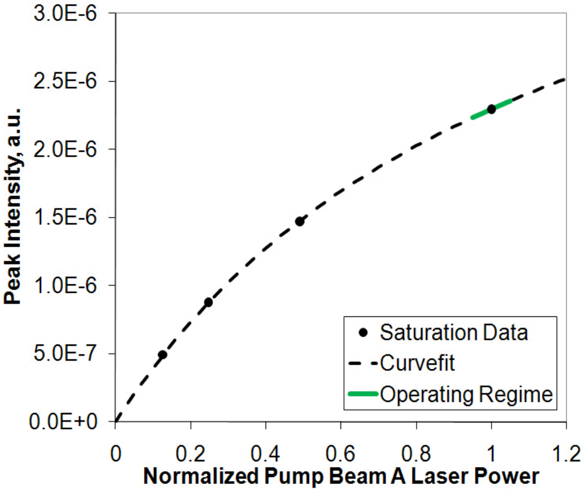

Figure 5. Saturation study plot for IM-LIF setup A

to the data based on Eq. 5, the saturation model equation. Each figure is also overlaid with solid colored lines indicating the approximate laser output at which all IMOG and IM-LIF traces were taken. From these two figures we can see the interrogated gas sample is well saturated by the input laser beams.

Figure 6 shows sample results for both IMOG and IM-LIF on the same plot for comparison. Except for the fact that one trace was collected using optogalvanic signal collection while the other was collected using fluorescence signal collection, the two raw traces were taken under identical conditions. The IMOG trace was taken immediately after the IM-LIF trace. Each trace took about 8 minutes to complete. The result shown in Fig. 6 indicates that optogalvanic signal collection produced far higher SNR than fluorescence signal collection. The optogalvanic signal was more sensitive to the saturation effect caused by the laser than the fluorescence signal. Furthermore, similar traces were taken with the focusing lenses in place. The signal became undetectable for IM-LIF so no more fluorescence based data were taken.

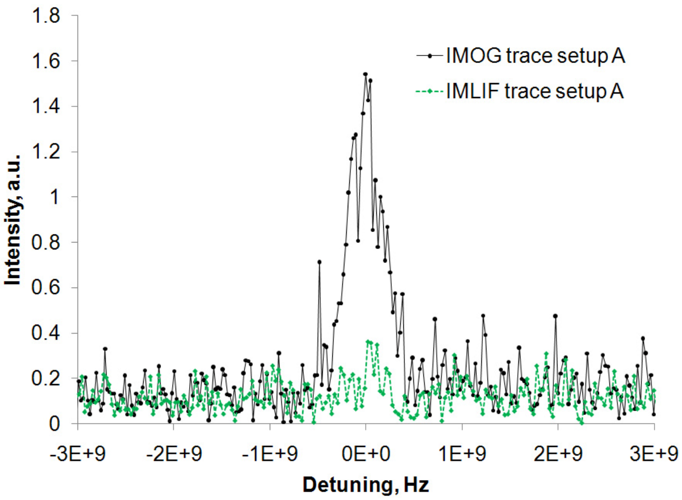

Figure 6. Raw data comparison between IMOG and IM-LIF

Studies were also done comparing data taken at the sum of the two beams' chopping frequencies as oppose to at the difference of the frequencies; data taken at the sum of frequencies consistently show roughly an order of magnitude better SNR. This may have been due to the fact that the difference of frequencies is ~190 Hz, where environmental electrical interference could have been an issue. All data presented were collected at the sum of chopping frequencies.

B. IMOG Results as a Function of Saturation Level

As a part of the experiment for setup A, two focusing lenses were added and removed from the lens train to study the effect of greatly boosting the degree of saturation without changing the total laser power. Figure 7 is the saturation study plot associated with having the focusing lenses in place. Note the level of saturation is higher when compared to Fig. 4.

Figure 8 compares an IMOG trace taken with the focusing lenses in place against a trace taken without the lenses. Figure 8 shows that the SNR actually went to near zero with the focusing lenses in place, which is contrary to what our original expectations. This is most likely because placing the focusing lenses also changed the size of the interrogation zone, greatly decreasing the number of particles being interrogated. Additionally, two thin beams are

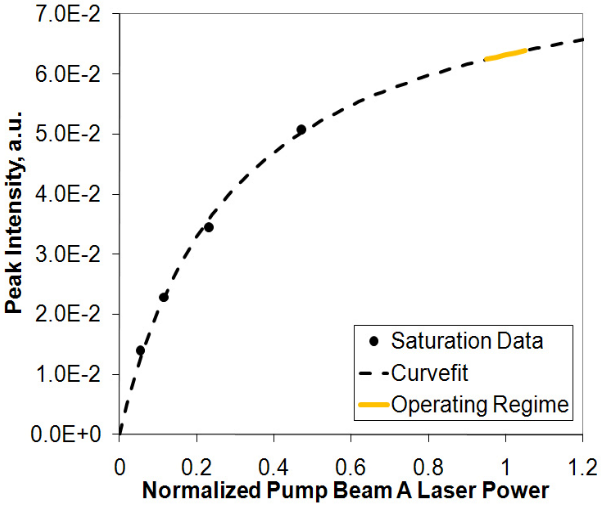

Figure 7. Saturation study plot for IMOG with focusing lenses in place

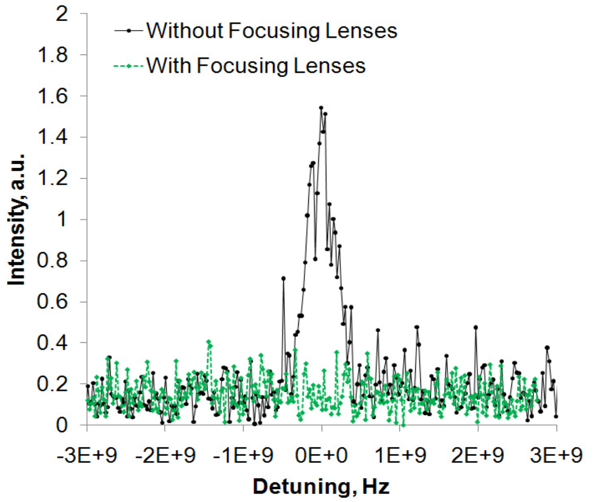

Figure 8. Raw IMOG traces taken with and without the focusing lenses in place for setup A

more difficult to line up and may have contributed to the signal not being detectable. This discovery inspired experimental setup B where the saturation level is easy to tweak through the aid of a variable neutral density filter. The interrogation region remains the same regardless of the saturation level. The downside is that the saturation level and the laser power level are changed simultaneously.

Figure 9 shows the saturation study plot for data taken with setup B. Unlike the preceding saturation study plots, IMOG data were taken at different saturation levels along this saturation plot. The exact laser power levels at which traces were taken are marked as crosses, which roughly correspond to 40, 60, 80, and 100 percent of available laser power. Available laser power was measured for pump beam A at 25.5±0.5 mW while the chopper is running.

Four IMOG traces were taken at each of the said power levels and averaged to obtain a kernel. Each trace used a lock-in time constant of 1 second and data was collected at the sum of the two chopper frequencies. Data was also taken at 20 percent of full power but the SNR was too low for the traces to be useful. The traces were averaged by first finding the mean frequency of the trace in order to line them all up with respect to each other. Then, the traces were merged and every four data points averaged to obtain a kernel. Figure 10 shows the averaged results of the four data sets plotted together. From Fig. 10, we see that while the FWHM of the Doppler-free scans goes down as the sample becomes less saturated, the SNR also worsens. Table 1 summarizes the FWHM and SNR value for each of the four data sets. The 40-percent-laser-power trace (dotted line in Fig. 10) is ~15% thinner than the full-power trace but the scan is so much noisier that it is difficult to determine whether the features are noise or real hyperfine structures.

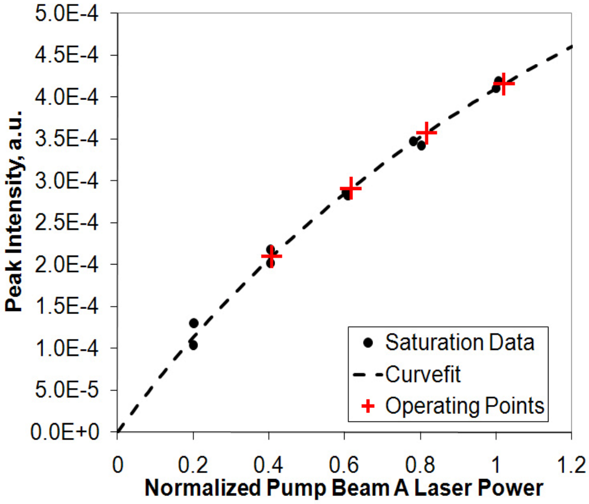

Figure 9. Saturation study plot for IMOG data taken with setup B

Table 1. Summary of IMOG results as a function of input laser power

Data Set	Average pump beam A laser power, mW	Approx. percent of full power	FWHM, MHz	SNR
1	26.1	100%	449	15.0
2	20.9	80%	447	11.6
3	15.8	60%	421	7.5
4	10.4	40%	373	5.8

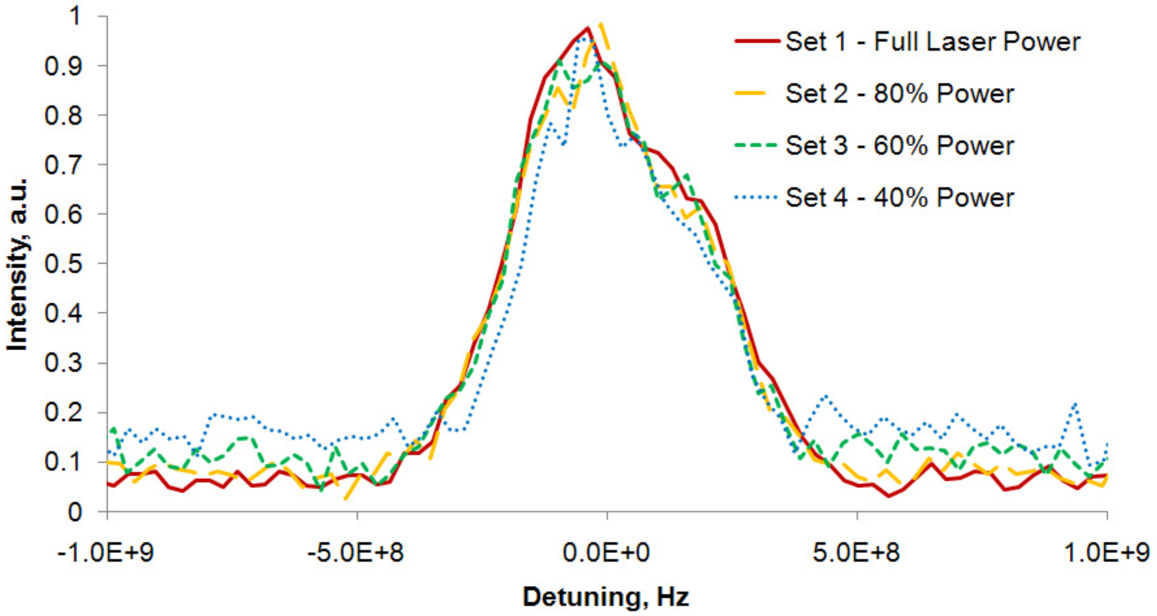

Figure 10. IMOG results by input laser power level; pump beam A at ~26 mW corresponds to full power

As a compromise between increasing SNR and decreasing saturation broadening, a set of 7 scans were taken with pump beam A laser power at ~14 mW. This corresponds to ~55% of full power on Fig. 9. The averaged result was then smoothed with a seven-point Savitzky-Golay filter.[11] Lastly, the noisy floor away from the peak was removed by linearly extrapolating for where the two slopes of the peak meets the horizontal zero axis. The final result, which is considered to be the best obtainable with the current setup, is shown in thick solid black line in Fig. 11. This final result will be referred to as the IMOG kernel for the remainder of the paper. Also shown in Fig. 11 in thin solid line is a normal (non-saturation broadened) optogalvanic trace taken under the same optogalvanic cell operating condition as was used to obtain the IMOG spectra. From previous measurements of xenon lines with known hyperfine structure constants it is determined that the gas temperature is 600±50 K at this operating condition. A red dash curve showing a simulated 600 K predicted spectrum is shown in Fig. 11; this spectrum is obtained by convolving the IMOG kernel with a 600 K Maxwellian velocity distribution. The normal optogalvanic trace and the simulated 600 K trace based on the obtained kernel shows excellent agreement. The simulated spectrum is slightly broader than the normal optogalvanic trace mostly because some Doppler broadening remains in the obtained kernel. Even a small amount of Doppler broadening can smooth out sharp hyperfine features that are packed closely together. This is why the IMOG kernel does not look like a series of spikes. The IMOG kernel has a FWHM of ~440 MHz; most of the strong hyperfine lines should lie within that confine. This kernel does not capture the wings of the hyperfine structure lineshape perfectly since the wings are composed of weak, relatively unsaturated hyperfine splittings. Nevertheless, it is usable for deconvolution purpose. Section V will put an upper bound on how much uncertainty is introduced when using this IMOG kernel.

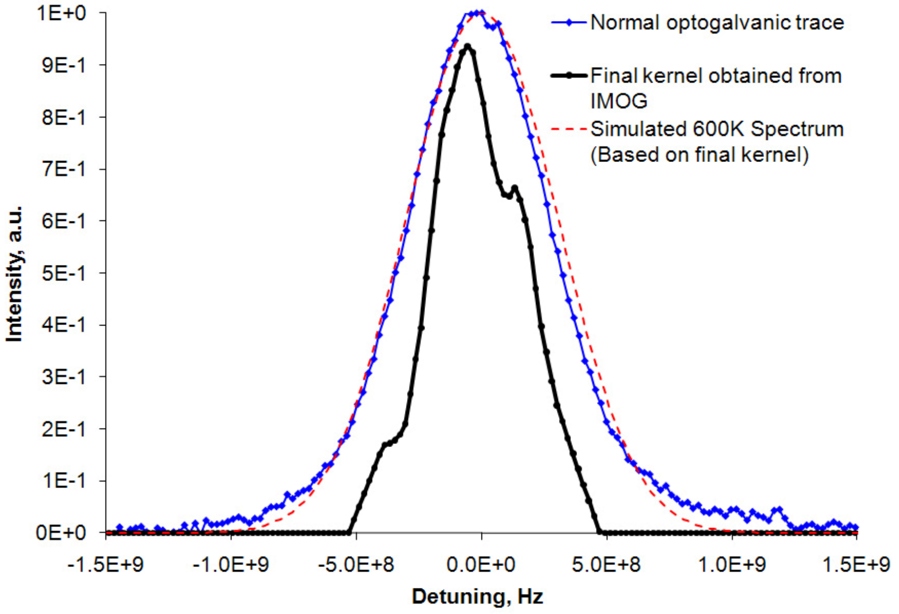

Figure 11. Final kernel obtained from IMOG tests; a normal spectra and simulated spectra based on the kernel are also shown for comparison

V. Validation and Uncertainty Analysis

The LIF data used to perform validation and uncertainty analysis were taken in a separate test on the 6-kW Hall thruster shown operating in Fig. 12. The experimental setup is very similar to that described in a previous paper.[5] However, the collection optics was set at an angle with respect to the exit plane of the thruster so that it is possible to collect LIF data from the inside of the Hall thruster channel. Details about the LIF experiment will be published in a future paper.[12] The data to be shown here were obtained on thruster channel centerline at different locations along its firing axis. The thruster was operating at its nominal condition of 300 V discharge voltage and 20 mg/s anode mass flow rate. This data set spans the entire acceleration zone of the thruster at this operating condition and thus gives a good coverage of the various types of velocity distribution functions that are found in this Hall thruster.

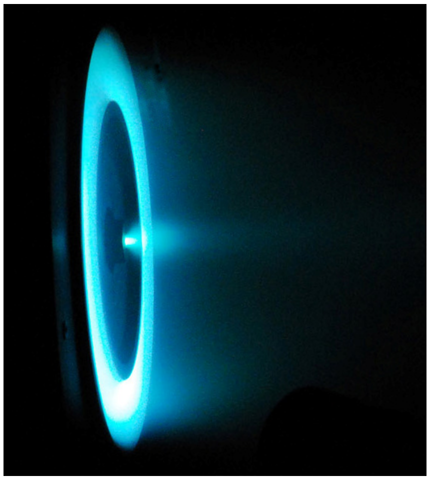

Figure 12. 6-kW Hall thruster in operation

Deconvolution was carried out using fast-Fourier transform the exact method of which is described in great detail by Smith.[13] The code used to carry out this deconvolution routine discretize the lineshape into points evenly spread in frequency space and also applies a Gaussian smoothing filter to remove some of the noise. In addition to the IMOG kernel, shown in Fig. 11, a simple Dirac delta function was also prepared as a kernel, which will be refer to as the placebo kernel. Deconvolving out a Dirac delta function is mathematically the same as assuming no hyperfine structure and no natural broadening. But by running the deconvolution routine with this placebo kernel we get the same level of discretization and smoothing as when deconvolving out the IMOG kernel. This procedure is necessary if we want to compare the results between taking and not taking hyperfine structures into account.

Figure 13 compare the VDF results obtained using the IMOG kernel (solid black line) and the placebo kernel (dashed blue line). The raw LIF data for Fig. 13 was obtained at 15 mm inside the thruster channel where particles were almost stationary. Figure 14 is a similar comparison plot for data obtained at the exit plane of the thruster channel where high amplitude plasma oscillations caused significant broadening to the time-averaged VDF. From both plots, we see that the difference in the obtained results is small. However, the differences are more pronounced in Fig. 13 because the spread of particle velocities is much smaller for plasma deep inside the thruster than for plasma around the exit plane. Also, we can see that the features in the VDF tend to be more distinct when the IMOG kernel was used, though the noise peaks are also sharper. Note that in Fig. 13, taking the hyperfine structures into account reveals a small double-hump at the top of peak, whereas the result from using the placebo kernel shows one smooth peak. It is not entirely clear from looking at Fig. 13 and 14 why taking the hyperfine structure into account is advantageous; we need to look at a more detailed numerical analysis.

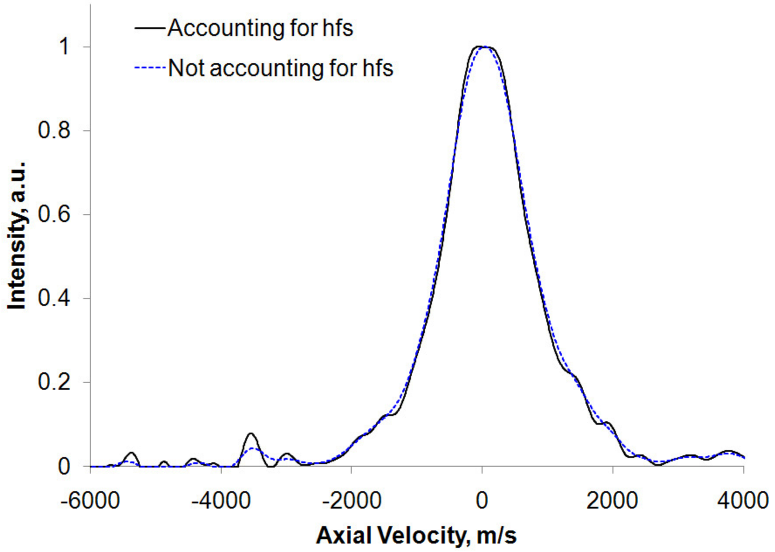

Figure 13. Comparison of VDF obtained at 15 mm into the channel a Hall thruster while taking and not taking hyperfine structures into account; hfs stands for hyperfine structures

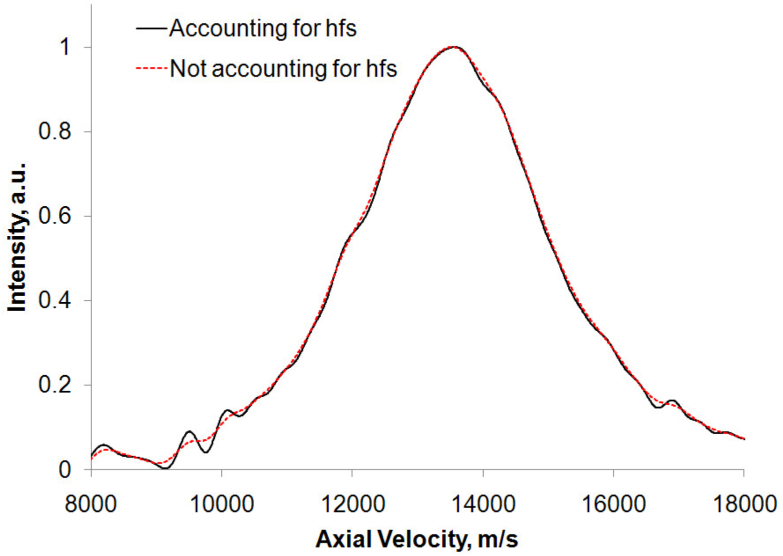

Figure 14. Comparison of VDF obtained at the exit plane of a Hall thruster while taking and not taking hyperfine structures into account

Table 2 lists a number of physical parameters extracted from the VDFs that were obtained from various axial locations in the thruster channel. Note that a location of 0 mm marks the exit plane of the thruster and negative location values are inside the thruster channel. Maxwellian temperatures are also calculated for distributions that are roughly stationary (defined as bulk velocity is less than 10% of fully accelerated velocity). Temperatures are not given for other VDFs because they are distinctly non-Maxwellian. From this table we can readily see the difference in the results obtained with the IMOG and the placebo kernels. There is negligible difference in the obtained bulk velocities. For the near-stationary VDFs, using the placebo kernel results in FWHM velocities that are 4-6% higher than using the IMOG kernel, which translates to temperatures that are 8-13% higher. However, for the accelerating plasma where various factors like plasma oscillation broadens out the VDF, only a 1-4% difference is seen in the FWHM velocities. Since we know the IMOG kernel is not perfectly Doppler-free, using it must reduce the width of a VDF too much so that the true FWHM velocity lies somewhere between the results from using the two kernels. Thus the difference percentages above are also upper bounds on the uncertainty associated with using the IMOG kernel. It is very likely the true solution lies much closer to that obtained using the IMOG kernel, but without better Doppler-free traces it is difficult to say how much closer. Figure 15 shows the various VDFs obtained at the locations listed in Table 2 using the deconvolution methodology described in this paper.

Table 2. Comparison of physical parameters obtained with and without taking hyperfine structure into account

Axial location, mm	**Deconvolution using IMOG kernel**			**Deconvolution ignoring hyperfine effects**			**Percentage difference in**		
	Bulk velocity, m/s	**FWHM velocity, m/s**	**Temp-erature, K**	**Bulk velocity, m/s**	**FWHM velocity, m/s**	**Temp-erature, K**	**Bulk velocity**	**FWHM velocity**	**Temp-erature**
-15	**132**	**1413**	**5690**	**130**	**1468**	**6140**	**-1.74%**	**3.9%**	**7.9%**
-12	**400**	**1242**	**4390**	**402**	**1321**	**4970**	**0.50%**	**6.4%**	**13.1%**
-9	**944**	**1431**	**5830**	**943**	**1499**	**6400**	**-0.11%**	**4.8%**	**9.7%**
-6	**2490**	**2483**		**2493**	**2545**		**0.12%**	**2.5%**	
-3	**6425**	**3890**		**6425**	**4043**		**0.00%**	**3.9%**	
0	**13625**	**3321**		**13628**	**3321**		**0.02%**	**0.0%**	
3	**15854**	**2740**		**15857**	**2795**		**0.02%**	**2.0%**	
6	**17449**	**2771**		**17451**	**2838**		**0.01%**	**2.4%**	
9	**18245**	**2691**		**18248**	**2722**		**0.02%**	**1.2%**	
12	**18778**	**2483**		**18777**	**2508**		**-0.01%**	**1.0%**	
15	**19091**	**2257**		**19092**	**2294**		**0.01%**	**1.6%**	

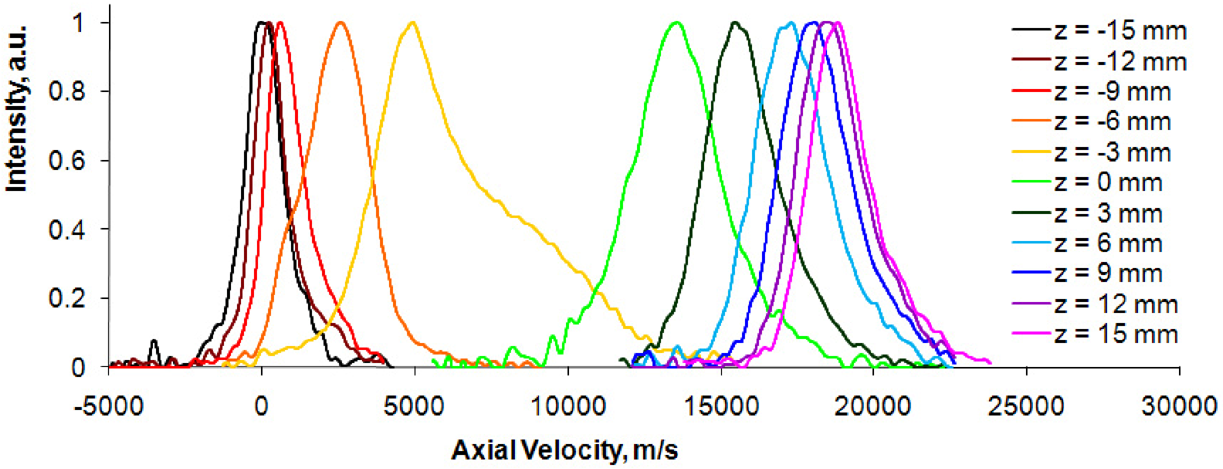

Figure 15. VDFs obtained from 6-kW Hall thruster operating at nominal condition

VI. Conclusion

Although the Xe II $5d[4]_{7/2} \rightarrow 6p[3]^{o}_{5/2}$ transition line contains unknown hyperfine structure constants, we have shown that it is still possible to extract velocity distribution functions from laser-induced fluorescence data obtained with this line. The intermodulated experiments described in this paper yielded a slightly Doppler-broadened hyperfine line structure. While hyperfine structure constants cannot be obtained from this result, directly deconvolving this result from the LIF data yielded more distinct features than not deconvolving out the hyperfine structures out at all. Furthermore, application of this deconvolution approach is more important for plasma with smaller spreads in velocities like those found inside the thruster channel than for plasma with larger spreads like those found at the exit plane and beyond. Not removing the hyperfine structure could cause over 10% error in temperature measurement, not to mention inaccurately calculating the shapes of the velocity distribution functions. The uncertainty analysis showed that for the part of the Hall thruster channel where most of the acceleration occurs, the maximum error in FWHM velocity is ~4% and the error in bulk velocity is ±0.1%.

Other applications of this technique are highly situation dependent. For example, we could have alternately obtained seven samples for the seven dominant isotopes of xenon and map out the individual isotopic shift. But while having actual hyperfine structure constants is more preferable, it is far more economical, under circumstances like those described in this paper, to directly trace the hyperfine structure and deconvolve it from the LIF data.

Acknowledgments

The authors would like to acknowledge and thank the Air Force Office of Scientific Research (AFOSR) for funding this research. Dr. Mitat Birkan is the Project Manager for Grant FA9550-06-1-0105.

References

[1] Hargus, W. A., Jr. and Cappelli, M. A., "Laser-Induced Fluorescence Measurements within a Laboratory Hall Thruster", *30th Plasmadynamics and Lasers Conference*, AIAA-1999-3436, Norfolk, VA, 28 Jun. - 1 Jul., 1999.

[2] Smith, T. B., Ngom, B. B., Linnell, J. A., and Gallimore, A. D., "Diode Laser-Induced Fluorescence of Xenon Ion Velocity Distributions", *41st AIAA/ASME/SAE/ASEE Joint Propulsion Conference*, AIAA-2005-4406, Tucson, AZ, 11-13 Jul., 2005.

[3] Hargus, W. A., Jr. and Charles, C. S., "Near Exit Plane Velocity Field of a 200-Watt Hall Thruster", *Journal of Propulsion and Power*, Vol. 24, No. 1, Jan.-Feb., 2008, pp. 127-133.

[4] Hargus, W. A., Jr. and Charles, C. S., "Near Plume Laser Induced Fluorescence Velocity Measurements of a 600 W Hall Thruster", *44th AIAA/ASME/SAE/ASEE Joint Propulsion Conference & Exhibit*, AIAA-2008-5004, Hartford, CT, 21-23 Jul., 2008.

[5] Huang, W., Reid, B. M., Smith, T. B., and Gallimore, A. D., "Laser-Induced Fluorescence of Singly-Charged Xenon in a 6-kW Hall Thruster Plume", *44th AIAA/ASME/SAE/ASEE Joint Propulsion Conference & Exhibit*, AIAA-2008-5102, Hartford, CT, 21-23 Jul., 2008.

[6] Gawron, D., Mazouffre, S., Sadeghi, N., and Heron, A., "Influence of Magnetic Field and Discharge Voltage on the Acceleration Layer Features in a Hall Effect Thruster", *Plasma Sources Science and Technology*, Vol. 17, 025001, 2008.

[7] Mazouffre, S., Pawelec, E., Bich, N. T., and Sadeghi, N., "Doppler-Free Spectroscopy Measurements of Isotope Shifts and Hyperfine Components of Near-IR Xenon Lines", *American Institute of Physics Conference Proceedings*, 2006.

[8] Svanberg, S., *Atomic and Molecular Spectroscopy*, 4th ed., Springer-Verlag, Berlin, 2004.

[9] Harkness, H. W. and Heard, J. F., "The Stark Effect for Xenon", *Proceedings of the Royal Society of London. Series A, Containing Papers of a Mathematical and Physical Character*, Vol. 139, No. 838, 1 Feb., 1933, pp. 416-435.

[10] Smith, T. B., Huang, W., Ngom, B. B., and Gallimore, A. D., "Optogalvanic and Laser-induced Fluorescence Spectroscopy of the Zeeman Effect in Xenon", *30th International Electric Propulsion Conference*, 2007-229, Florence, Italy, 17-20 Sep., 2007.

[11] Savitzky, A. and Golay, M. J. E., "Smoothing and Differentiation of Data by Simplified Least Squares Procedures", *Analytical Chemistry*, Vol. 36, No. 8, Jul., 1964, pp. 1627-1639.

[12] Huang, W., Drenkow, B., and Gallimore, A. D., "Laser-Induced Fluorescence of Singly-Charged Xenon Inside a 6-kW Hall Thruster", *45th AIAA/ASME/SAE/ASEE Joint Propulsion Conference & Exhibit*, AIAA-2009-5355, Denver, CO, 2-5 Aug., 2009 (to be published).

[13] Smith, T. B., "Deconvolution of Ion Velocity Distributions from Laser-Induced Fluorescence Spectra of Xenon Electrostatic Thruster Plumes", Ph.D. Dissertation, Aerospace Engineering, University of Michigan, Ann Arbor, MI, 2003.